PCCP

# Nuclear dynamics in quantum clusters†

**Andreas Heidenreich, Isidore Last, Uzi Even and Joshua Jortner***

*School of Chemistry, Tel-Aviv University, Ramat Aviv, 69978 Tel Aviv, Israel*

***Received 15th January 2001, Accepted 6th April 2001***
***First published as an Advance Article on the web 18th May 2001***

We address recent developments in the exploration of quantum nuclear dynamics in large, finite, low-temperature systems, focusing on Bose–Einstein condensates ($T \simeq 100$ nK), optical molasses ($T \simeq 10$–$100$ μK) and aromatic molecule · $He_n$ clusters ($T = 0.4$ K). The expansion of optical molasses bears a close analogy to the nuclear dynamics of Coulomb explosion of multicharged clusters. Spectroscopy of electronic–vibrational excitations of anthracene · $He_n$ clusters manifests large nuclear quantum effects, nonrigidity, large scale confinement and permutational symmetry effects. Perspectives for the novel research area of nuclear dynamics of ultracold finite systems are advanced.

## I. Prologue

Cluster chemical physics[1–3] focuses on the structure, energetics, electronic level structure, spectroscopy, dynamics, chemical reactivity and function of large finite systems. Recent developments in the explorations of new systems and concepts advanced on the basis of cluster science (Fig. 1) encompass the novel research areas of nanoparticles and mesoscopic systems,[4] ultracold finite clouds[5–7] and finite quantum systems.[8–12] The response and dynamics of nanostructures, *e.g.* metal and semiconducting clusters, nanoparticles, nanotubes and quantum dots, constitute an interesting research area, striving towards the construction of single electron devices. An interesting direction is the utilization of single molecules, supramolecular systems, clusters and biostructures for the processing of electrical, optical, magnetic and chemical signals, providing the basis for molecular electronics.[13] The function of nanostructures rests on nuclear–electron or purely electron response and dynamics. Other fascinating phenomena in large finite systems pertain to the nuclear dynamics of ultracold systems[5–7,14,15] and nuclear quantum systems.[8–12]

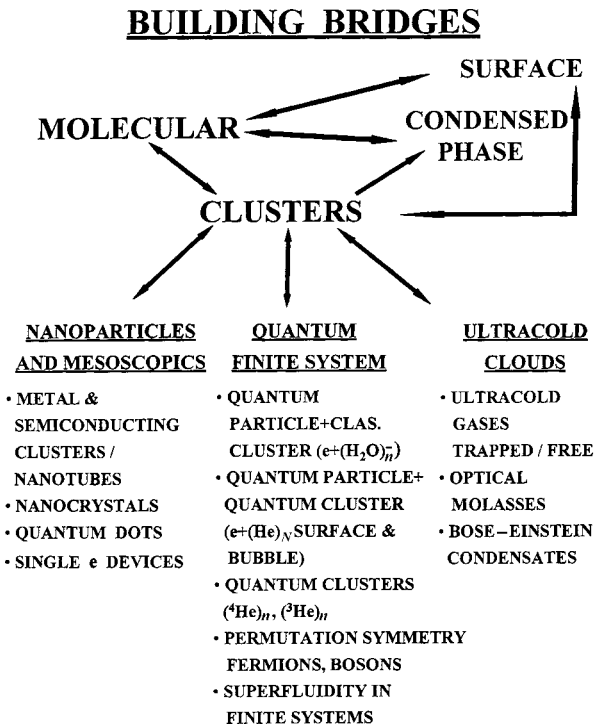


**Fig. 1** New large finite systems related to cluster science.

## II. Some facets of nuclear dynamics of ultracold systems

A fascinating new research area focuses on phase transitions, spectroscopy and nuclear dynamics of finite ultracold gases in the low-temperature domain of $T = 100$ nK–100 μK.[5–7,15] These involve gases in magneto-optical traps, optical molasses[5–7] and Bose–Einstein condensates.[15] Pruvost, Serre, Duong and Jortner[7] established a remarkable analogy between the nuclear dynamics of the expansion of ultracold optical molasses[5–7] and the Coulomb explosion of molecular clusters.[16,17] Coulomb explosion of highly charged molecular clusters, *e.g.* $(Xe^{+q})_n$ ($q = 1$–$8$ and $n = 10$–$1000$) or $(D^+)_n$ ($n = 100$–$1000$),[17] which is induced by multielectron ionization in ultra-intense laser fields (intensity $I = 10^{15}$–$10^{18}$ W cm$^{-2}$), is characterized by ultrafast time scales (10–100 fs) and ultrahigh energies for nuclear motion (ion energies in the range of 1 keV–1 MeV, corresponding to the energy domain of nuclear physics). The characteristic time scale for cluster Coulomb explosion is[16] $\tau_{EX} \propto q^{-1} m^{1/2} R_0^{3/2}$, where $q$ is the individual ionic charge, $m$ its mass and $R_0$ the interionic separation, with $\tau_{EX}$ being independent of the initial cluster size. Typical values for $(Xe^+)_n$ clusters with $q = 1$, $m = 131$ u and $R_0 = 3.5$ Å are $\tau_{EX} \simeq 100$ fs. We now proceed to nuclear dynamics of optical molasses.[7] These involve a cloud of trapped neutral atoms, *e.g.* Rb, which is characterized by a density of $\rho = 10^{10}$–$10^{11}$ cm$^{-3}$ in a magneto-optical trap, with the magnetic field being suppressed as the cloud expands *via* the radiative trapping force. This radiative trapping force, originating from photon emission and reabsorption between pairs of atoms separated by a distance $r_{12}$, is proportional[5–7] to $r_{12}^{-2}$ (with an effective charge $q$). Accordingly, the radiative trapping force is analogous to the Coulomb law, and the expansion of the cloud is isomorphous to cluster Coulomb explosion. In scaling of the cluster Coulomb explosion lifetime

† Dedicated to Professor Jürgen Troe on his 60th birthday.

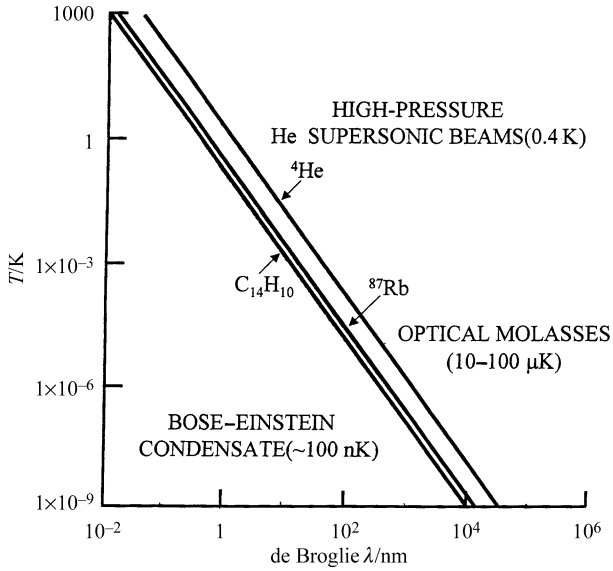


**Fig. 2** The temperature dependence of the thermal de Broglie wavelength for several atomic and molecular systems. The relevant temperature domains for Bose–Einstein condensates, optical molasses and clusters containing $^4$He are marked on the figure.

$\tau_{EX}$ given above to obtain the time scale $\tau_M$ for the expansion of the optical molasses of Rb (with $q = 10^{-5}$ e, $m = 87$ u and $R_0 = 10^{-4}$ cm), Pruvost *et al.*[7] set $\tau_M = \mathscr{F}\tau_{EX}$, where the scaling factor is[7] $\mathscr{F} \simeq 10^{10}$. This courageous extrapolation[7] results in $\tau_M \simeq 1$ ms for the expansion of optical molasses. This prediction is in good agreement with recent experimental data,[7] where the expansion of cooling of bright three-dimensional optical molasses of Rb is characterized by a time scale of 1.4 ms, and occurs in the (translational) temperature domain of $T_M = 100$–$10$ μK.

Another interesting example for the nuclear dynamics of ultracold, large, finite systems pertains to the molecular description of Bose–Einstein condensation of atoms with a negative scattering length, *e.g.* $^7$Li atoms confined in a harmonic trap[14,15] at $T \simeq 100$ nK. Bohn *et al.*[14] have shown that this system can be treated by a transformation to a hyperspherical collective coordinate, resulting in a set of coupled differential equations, whose decoupling in terms of the K harmonic approximation results in a one-dimensional effective potential for collective nuclear motion. For a negative atomic scattering length the effective potential contains only metastable states subjected to macroscopic tunneling. For an assembly of $^7$Li atoms practical stability is insured for a critical size of $N_{CR} \simeq 1400$.[15] These examples manifest the novel features of the nuclear dynamics of finite ultracold systems.

A simple, but useful, physical representation of nuclear quantum effects in ultracold finite systems is given in Fig. 2, where we present the temperature dependence of the thermal de Broglie wavelength $\lambda = h/(2mk_BT)^{1/2}$ and mark the relevant temperature domain for several characteristic systems, *e.g.* Bose–Einstein atomic condensates ($T \simeq 100$ nK, $\lambda \simeq 10^3$ nm), and $^{87}$Rb optical molasses ($T = 10$–$100$ μK, $\lambda \simeq 10^2$ nm).

## III. Nonrigid helium clusters

Proceeding to a higher temperature domain ($T \simeq 0.4$ K), we encounter the world of finite quantum nuclear clusters (Fig. 2). Landmark examples involve $(^4He)_n$ ($n \geqslant 2$) and $(^3He)_n$ ($n \geqslant 25$) quantum clusters ($\lambda = 1$ nm at 0.4 K), which exhibit large scale zero-point energy motion and manifest boson (for $^4$He) or fermion (for $^3$He) permutational symmetry.[8] Of considerable interest in this context is the phenomenon of superfluidity in finite $(^4He)_n$ boson clusters, which was explored by Toennies *et al.*[8–10,12] in the temperature range 0.4–0.2 K. Other, closely related, finite quantum systems involve van der Waals clusters of $^4$He atoms bound to aromatic molecules.[18–32] The exploration of aromatic molecule–rare gas clusters was initiated 20 years ago.[33] Notable studies of benzene · $He_n$ ($n = 1$, 2)[19,32] and naphthalene · $He_1$ (ref. 30) provided information on the van der Waals bond lengths and nuclear vibrational excitations. The recent spectroscopic interrogation of the anthracene · $He_n$ and tetracene · $He_n$ 'quantum clusters' at $T = 0.4$ K performed by Even *et al.*[31] allows for the experimental and theoretical exploration of some of their unique features:

(1) *Large nuclear quantum effects.* In these systems, *e.g.* heteroclusters containing He atoms on aromatics, $\lambda \gtrsim d$. The de Broglie wavelength ($\lambda$) is comparable to, or exceeds, the characteristic length ($d$), *e.g.* the bond length of the rigid subsystem.

(2) *Nonrigidity.* Both neat $(He)_n$ clusters and heteroclusters containing He atoms remain nonrigid down to $T = 0$, *e.g.* $(He)_n$ clusters remain liquid at zero temperature. He–aromatic molecule heteroclusters exhibit large-scale nuclear motion at $T = 0$, being dominated by large zero-point energy effects.

(3) *Large-scale confinement.* The large-amplitude nuclear motion in $He_n$–aromatic molecule clusters is confined horizontally by the nuclear framework of the aromatic molecule and vertically by the restoring force of the aromatic microsurface.

(4) *Effects of permutational nuclear symmetry.* In these systems the function[34] $\exp(-d^2/\lambda^2)$ assumes the values $\sim 1$. Accordingly, the effects of boson (for $^4$He) or fermion (for $^3He_n$) permutational symmetry are important.[34]

The implication of large nuclear quantum effects, nonrigidity and large-scale confinement in aromatic molecule · $He_n$ heteroclusters manifest spatial nuclear delocalization in floppy cluster systems, where the traditional chemical concept of structure breaks down. He delocalization in excited vibrational states of 2,3-dimethylnaphthalene · $He_1$ clusters over the aromatic microsurface was inferred by Bach *et al.*[30] Our studies of larger aromatic microsurfaces, *e.g.* anthracene · $He_n$ ($n = 1$, 2), reveal extensive spatial delocalization of He atoms at the ground vibrational state, in both the $S_0$ and $S_1$ electronic states, bringing up the notion of nonrigid large molecular clusters. While the traditional concept of 'rigid' molecular (and cluster) structures constitutes a cornerstone for stereochemistry and for spectroscopy, the limitations of this traditional concept emerged from probing quantum states of matter, with early examples being the inversion of ammonia and the pseudorotation of cyclopentane.[35] Stationary states of molecules or clusters must contain the permutation symmetry for all identical nuclei.[35] For nonrigid clusters, *e.g.* the aromatic molecule · $(He)_n$, whose $(He)_n$ subpart is devoid of structure even at 0 K, the symmetry of the nuclear Hamiltonian (within the framework of the Born–Oppenheimer separation of electronic and nuclear motion and for a spatially fixed aromatic molecule) is determined by the symmetry of the confining rigid nuclear framework of the aromatic molecule and by the permutation group of the indistinguishable He nuclei.

## IV. Spectroscopy and nuclear dynamics of anthracene · $He_n$ clusters

In our analysis of the energetics and nuclear dynamics of aromatic molecule–He clusters we shall rely on information from electronic–vibrational spectroscopy to make inferences about the geometries and topologies of the nuclear potential surfaces and the quantum states of these floppy clusters. Even *et al.* developed[31] experimental methods for the cooling of large molecules and clusters in pulsed (10 μs) high pressure (100 atm) supersonic He jets down to a low temperature of 0.4 K. Rotational thermometry of aniline[31] and of anthracene[31] in these pulsed high pressure jets resulted in the rotational temperature of $T_R = 0.4 \pm 0.1$ K for both large molecules. The

low (0.4 K) temperature thus accomplished[31] constitutes, to the best of our knowledge, the current low-temperature record for the spectroscopic interrogation of large molecules and clusters in supersonic jets. This technique was applied[31] to the electronic–vibrational spectroscopy of anthracene · $He_n$ and tetracene · $He_n$ ($n = 1$–10). The $S_0 \rightarrow S_1$ excitation spectra of anthracene · $He_n$ clusters obtained from two-color two-photon excitation-ionization[31] are displayed in Fig. 3. Two interesting experimental results emerge:

(i) *Anomalous spectral shifts of the $S_0 \rightarrow S_1$ electronic origin.* The spectral shifts $\delta\nu_n$ of the electronic origin of anthracene · $He_n$ ($n = 1$–10) clusters, which correspond to the lowest energy excitation of each mass-selected cluster (Fig. 4) are to the red, manifesting the dominance of dispersive interactions for $\delta\nu$. The $n = 1$ cluster reveals a low value of $\delta\nu_1 = -1.6$ cm$^{-1}$, which is attributed to the one-sided (1|0) structure. The $n = 2$ cluster, with $\delta\nu_2 = -3.2$ cm$^{-1}$, is assigned to the two-sided (1|1) cluster in view of the additivity relation $\delta\nu_2 = 2\delta\nu_1$. The large jump of $\delta\nu_3 = -12.6$ cm$^{-1}$ is attributed to the (2|1) structure for anthracene · $He_3$. Accordingly, we can estimate the spectral shift of the one-sided (2|0) structure as $\delta\nu(2|0) = \delta\nu(2|1) - \delta\nu(0|1) = -11.0$ cm$^{-1}$. The experimental spectral shift $\delta\nu_4 = -21.9$ cm$^{-1}$ for the $n = 4$ cluster is assigned to the two-sided (2|2) structure, with the experimental value of $\delta\nu_4$ being in accord with the estimate $\delta\nu(2|2) = 2\delta\nu(2|0) = -22.0$ cm$^{-1}$. Only two-sided structures are exhibited for $n > 1$. The anthracene · $He_n$ clusters reveal an irregular spectral shift, with an abrupt jump of $\delta\nu_n$ *vs.* $n$ at $n = 3$ (Fig. 4), which is manifested by the surprisingly large ratio $\delta\nu(2|0)/\delta\nu(1|1) = 3.47$. This behavior is in marked difference with spectral shifts of aromatic molecule–Ar, Kr or Xe clusters,[36] where the difference between the spectral shifts for the $n = 2$ (1|1) and (2|0) isomers is small. For example, for anthracene · $Ar_n$ clusters the difference in the spectral shifts for the one-sided and the two-sided structures is $\delta\nu(2|0)/\delta\nu(1|1) = 1.15$.[36] As we shall subsequently show, this dramatic large difference between the spectral shift for two-sided and one-sided structures of anthracene · $He_2$ originates from the large amplitude quantum motion of two He atoms on the microsurface of anthracene, which will change the balance between the dispersive and repulsive contributions to the spectral shift.

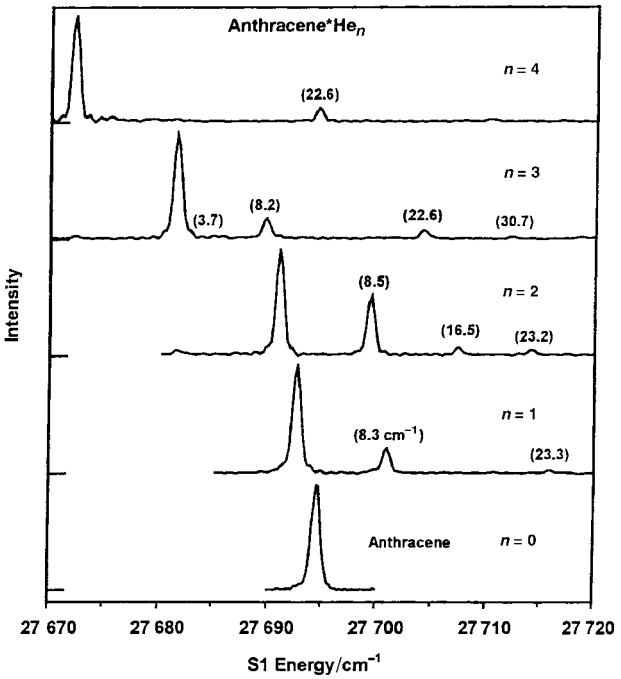


**Fig. 3** Excitation spectra from two-photon two-color ionization of anthracene · $He_n$ clusters ($n = 1$–4) at 0.4 K. The lowest energy spectral feature in each spectrum corresponds to the electronic origin. The spectrum marked $n = 0$ corresponds to the bare anthracene molecule.

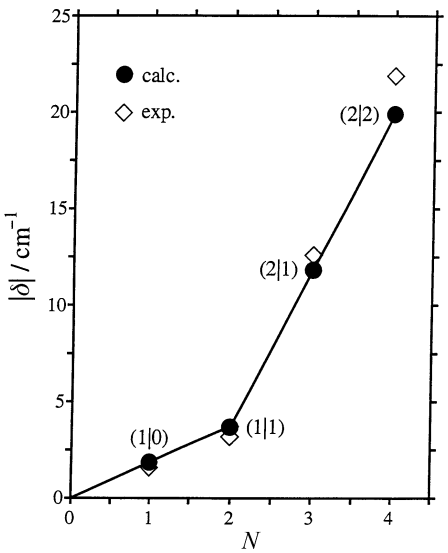


**Fig. 4** The spectral shifts of the electronic origin of the anthracene · $He_n$ ($n = 1$–4) clusters relative to bare anthracene. The relevant configurations (see text) are marked as ($m|m'$) with $m,m' = 1$ and 2. The experimental data (◇) are compared with the calculated (●) values (see text).

(ii) *The vibrational structure.* An extensive vibrational structure is exhibited at higher energies above the electronic origin (Fig. 3) of anthracene · He(1|0) ($n = 1$), anthracene · He(1|1) ($n = 2$) and anthracene · He(2|1) ($n = 3$) (Fig. 3). The vibrational frequencies are rather similar for $n = 1$ and 2. On the basis of the assignment of the spectral shifts [paragraph (i) above], we expect the vibrational level structure for the (1|0) ($n = 1$) and for the (1|1) structures to be identical. A notable exception is the additional spectral feature at 16.5 cm$^{-1}$ for the $n = 2$ (1|1) cluster, which cannot be accounted for at present. The vibrational structure manifests the energetics of the quantum states for the large amplitude nonrigid motion in these clusters.

## V. Theoretical exploration of small anthracene · He clusters

In our calculations of the energetics, spectral shifts and vibronic level structure of anthracene · $He_1$ and anthracene · $He_2$ clusters we kept the anthracene molecule rigid and spatially fixed. In the ground electronic state $S_0$ of anthracene, the anthracene · He potential $V_0$ was described in terms of a sum of atom–atom Lennard-Jones 6–12 potentials, with the potential parameters[37–39] being $\sigma_{C\text{-}He} = 2.74$ Å, $\varepsilon_{C\text{-}He} = 11.3$ cm$^{-1}$, $\sigma_{H\text{-}He} = 3.21$ Å and $\varepsilon_{H\text{-}He} = 4.2$ cm$^{-1}$. The anthracene · He potential $V_1$ in the $S_1$ electronically excited state of anthracene is given by $V_1 = V_0 + V_{DSS} + \Delta V_{LJ}$, where $V_{DSS}$ is the change in the dispersive energy between the $S_1$ and $S_0$ electronic states, which was calculated by the dispersive spectral shift theory of Shalev and Jortner[36,40] (with a scaling parameter[36,40] $\eta = 0.50$). The change $\Delta V_{LJ}$ in the repulsive Lennard-Jones interaction between $S_1$ and $S_0$, which was taken as $\Delta\sigma/\sigma_{C\text{-}He} = 0.065$ for the C9 and C10 carbon atoms of anthracene, were chosen (together with $\eta$) to fit the experimental spectral shift of anthracene · $He_1$. The He–He interaction potential was described in terms of a Morse potential fitting of the corresponding Lennard-Jones potential.[41] More elaborate He–He potentials[42] will be used in the future, but it appears that the present approximation is adequate for the two-particle He–He integrals.

The variational calculations for anthracene · $He_1$ utilized the (orthonormal) basis set $\phi_\mu(x,y,z) = \phi_{\mu x}(x)\phi_{\mu y}(y)\phi_{\mu z}(z)$,

where $x$, $y$ and $z$ are the in-plane short, the in-plane long and the perpendicular axes, respectively, with the center of mass of anthracene as the origin. Here $\phi_{\mu x}(x)$, $\phi_{\mu y}(y)$ and $\phi_{\mu z}(z)$ constitute the numerical solutions of the Schrödinger equation for one-dimensional cuts $V(x)$, $V(y)$ and $V(z)$ of the intermolecular potential $V_0(x,y,z)$, with $V(x)$ and $V(y)$ being taken for fixed $y = 0$ and $x = 0$, respectively, with the $z$ coordinate being optimized with respect to the minimal potential energy, while $V(z)$ was taken from $x = 0$ and $y = 0$. Our variational calculations for both the $S_0$ and $S_1$ electronic states with the wave function

$$\Psi(x,y,z) = \sum_{\mu=1}^{n} c_\mu \phi_\mu(x,y,z)$$

involved 165 3D basis functions.

For the anthracene · $He_1$ (1|0) configuration, the wave function for the vibrational ground state of $S_0$ consists almost exclusively of $\phi_{000}$ (coefficient 0.97), while in the $S_1$ state the vibrational wave function is subjected to a considerable admixture of higher $\phi_{xyz}$ wave functions, with the main components being $0.69\phi_{0,0,0} + 0.65\phi_{0,2,0}$, thus causing the probability density to flow towards the outer rings. While in the $S_0$ state the probability density

$$P(x,y) = \int_0^\infty \mathrm{d}z\, \psi^2(x,y,z)$$

of the He atom on the anthracene surface is mainly localized on the central ring, in the $S_1$ state the density is shifted towards the outer rings (Fig. 5). The He atoms are grossly delocalized (at $T = 0$) in both the $S_0$ and $S_1$ states. A measure of nonrigidity can be characterized by the standard deviation $\langle \Delta y^2 \rangle^{1/2}$ of $P(x,y)$ in the long-axis $y$ direction, which is 0.87 Å in $S_0$ and 1.76 Å in $S_1$. The vibrational excitations are classified according to the point symmetry of the (one-sided) anthracene microsurface. The vibrational level structure in the $S_0$ state (Fig. 6) reveals that for the lowest vibrational excitations in $S_0$ (5.3 and 8.5 $cm^{-1}$) thermal excitations are negligible under the experimental conditions ($T = 0.4$ K), emphasizing again the importance of low-temperature spectroscopy in these He clusters. The spectral shift is calculated from the difference of the lowest $1A_1$ state eigenvalues in the $S_1$ and $S_0$ electronic states (Fig. 6) as $\delta\nu = -1.9$ $cm^{-1}$ and is marked on Fig. 4. This spectral shift constitutes near-cancellation between moderately large dispersive, attractive (red shift) and repulsive (blue shift) contributions. Finally, we have calculated the energies and the nuclear Franck–Condon vibrational overlap factors for the allowed $S_0(1A_1) \rightarrow S_1(nA_1)$ electronic–vibrational excitations (Fig. 7). The prominent calculated vibrational excitations in $S_1$ originate from major contributions of $\phi_{0,\mu y,0}[y]$, $\phi_{\mu x,\mu y,0}[x,y]$ and $\phi_{0,0,\mu z}[z]$, $\phi_{0,\mu y,\mu z}[yz]$, where $[x]$, $[y]$ and $[z]$ denote the major contributions to the nuclear excitations from the corresponding one-dimensional functions. We assigned the experimental spectra (relative to the 0–0 origin) as: 8.3 $cm^{-1}$ $[y]$, 23.2 $cm^{-1}$ $[y]$, 37.2 $cm^{-1}$ $[y$ or $z]$ and 47.8 $cm^{-1}$ $[y$ or $yz]$. The calculated transition energies and the Franck–Condon factors are in reasonable agreement with experiment. This electronic–vibrational spectroscopy reflects on excitations of large scale nuclear motion in this cluster.

For the anthracene · $He_2$, one-sided (2|0) cluster, we have performed configuration interaction (CI) calculations with the nuclear wave functions consisting of a linear combination of

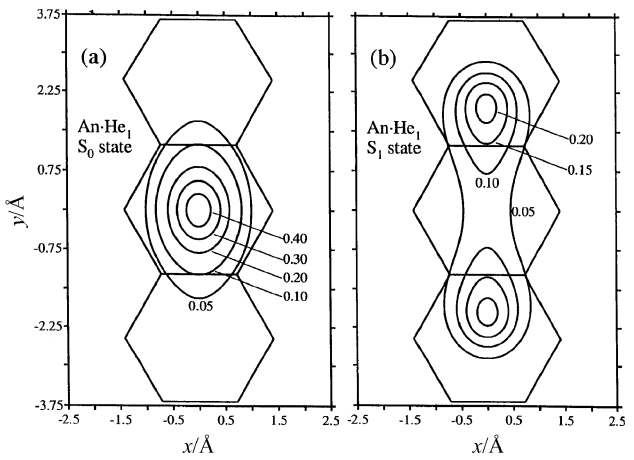


**Fig. 5** Contour plots of the probability density of the helium atom on the anthracene molecular surface for the vibrational ground state of anthracene · $He_1$: (a) the $S_0$ state; (b) the $S_1$ state.

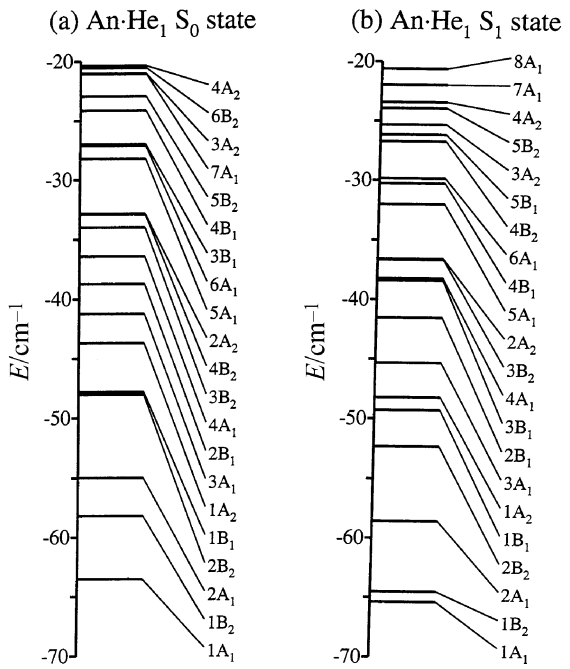


**Fig. 6** Vibrational level diagrams for the (1|0) configuration of anthracene · $He_1$: (a) the $S_0$ state; (b) the $S_1$ state.

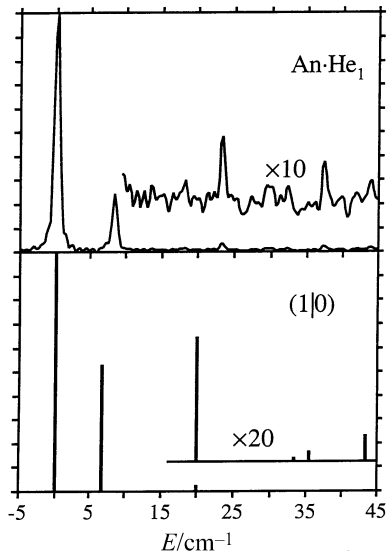


**Fig. 7** A comparison between the calculated and the experimental spectra for anthracene · $He_1$. The calculated vibronic lines (lower panel) are represented as sticks at the appropriate energies whose length, relative to the electronic origin, is proportional to the Franck–Condon factors.

symmetrized Hartree products $\Delta_\alpha(1,2)$, so that

$$\Psi(1,2) = \sum_\alpha c_\alpha \Delta_\alpha(1,2)$$

with 1 and 2 denoting the Cartesian coordinates of the helium atoms 1 and 2. All the one-particle and two-particle integrals were calculated numerically. The CI calculations involved 120 3D one-particle basis functions $\phi_{\mu x,\,\mu y,\,\mu z}(x,y,z)$, from which all possible ($\simeq$1800) Hartree products were generated and $\simeq 7 \times 10^6$ He–He integrals for each symmetry type of $C_{2v}$ anthracene microsurface were evaluated.

Due to He–He repulsion the delocalization of the He atoms in the anthracene$\cdot$He$_2$ (2|0) configuration is considerably more pronounced than for anthracene$\cdot$He$_1$. The measure of nonrigidity is given by $\langle\Delta y^2\rangle^{1/2} = 1.58$ Å for the $S_0$ and $\langle\Delta y^2\rangle^{1/2} = 1.93$ Å for the $S_1$ state. The markedly increased delocalization in the $S_1$ state results in the reduction of the contribution of the (blue) repulsive interactions and the enhancement of the contribution of the attractive (red) dispersive contributions to the spectral shift of the electronic origin. The calculated spectral shift for the (2|0) cluster, obtained from the difference of the lowest $1A_1$ state eigenvalues in $S_1$ and $S_0$, is $\delta\nu = -10$ cm$^{-1}$, being higher by a numerical factor of $\sim$5 than the corresponding spectral shift for the (1|0) cluster. Invoking additivity rules for anthracene$\cdot$He$_n$ ($n$ = 1–4) we used our theoretical results for the (1|0) and (2|0) clusters to calculate the spectral shift for the clusters $n$ = 2 (1|1), $n$ = 3 (1|2) and $n$ = 4 (2|2). The calculated spectral shifts (Fig. 4) account well for the abrupt jump in $\delta\nu$ *vs.* $n$ between $n$ = 2 and $n$ = 3, originating from the enhancement of dispersive interactions due to large amplitude parallel motion of the two He atoms located on one side of the microsurface of anthracene. The spectral shifts of the nonrigid He clusters arise from (small) contributions of mutually canceling dispersive and repulsive contributions, which result in very small (red) spectral shifts for the $n$ = 1 (1|0) and $n$ = 2 (1|1) clusters. The abrupt increase of the red spectral shifts for $n$ = 3 and $n$ = 4 manifests the consequences of the nuclear dynamics of two He atoms on one side of the aromatic microsurface, which involve the large scale nuclear motion (in both the $S_0$ and $S_1$ states) and the enhanced spatial delocalization (in the $S_1$ state) in these floppy clusters.

Cold (0.4 K) aromatic molecule$\cdot$He$_n$ clusters were interrogated by electronic $S_0 \rightarrow S_1$ excitations of the aromatic microsurface, which are coupled to the nuclear excitations of the nonrigid $(^4He)_n$ subsystem. These studies have to be extended in several directions. First, quantum time-resolved vibrational dynamics of these nonrigid systems will become amenable to experimental and theoretical investigation. Second, the exploration of the implications of permutational symmetry on the electronic–vibrational spectroscopy and nuclear dynamics of these quantum systems containing $^4$He and $^3$He will be of considerable interest. Third, collective nuclear excitations in aromatic molecule$\cdot(^4He)_n$ systems ($n > 5$), as interrogated by electronic–vibrational spectroscopy, may pave the way for the identification of the onset of superfluidity in finite, confined $(^4He)_n$ boson systems.[8–12]

## VI. Epilogue

We addressed some novel features of quantum nuclear dynamics in large, finite systems at low temperatures. Fascinating dynamic processes are expected to be manifested in the realm of the cold and ultracold world of large molecular and cluster systems (Fig. 8). We take (arbitrarily) the upper temperature limit for 'cold' systems ($T < 2.7$ K) to constitute the current temperature of the expanding universe, while the upper temperature limit for 'ultracold' systems is identified with the onset of cooling of atoms and molecules by optical methods ($T < 10^{-3}$ K). We have already discussed some features of the nuclear dynamics of Bose–Einstein condensates, optical molasses and He quantum clusters, which appear in Fig. 8, but there are many other, most interesting, systems and novel dynamic phenomena in this world (Fig. 8). Some dynamic molecular processes pertain to the photoassociation of alkali atoms to form ultracold diatomics,[43] cold collisions[44] and Auger ionization processes in a 'frozen' Rydberg gas.[45] Of considerable interest is nuclear dynamics accompanying 'phase transitions', *e.g.* a Bose–Einstein condensate of atoms[15] or superfluid $(^4He)_n$ clusters.[8–12] Nuclear quantum dynamics in these systems can be explored by the use of a spectroscopic probe [*e.g.* a dopant atom or molecule in $(^4He)_n$ clusters[10,11] or Bose–Einstein condensates] or a transport probe [*e.g.* the electron bubble in $(^4He)_n$ clusters].[10,11] Ultralow temperature nuclear dynamics will constitute a new scientific area.

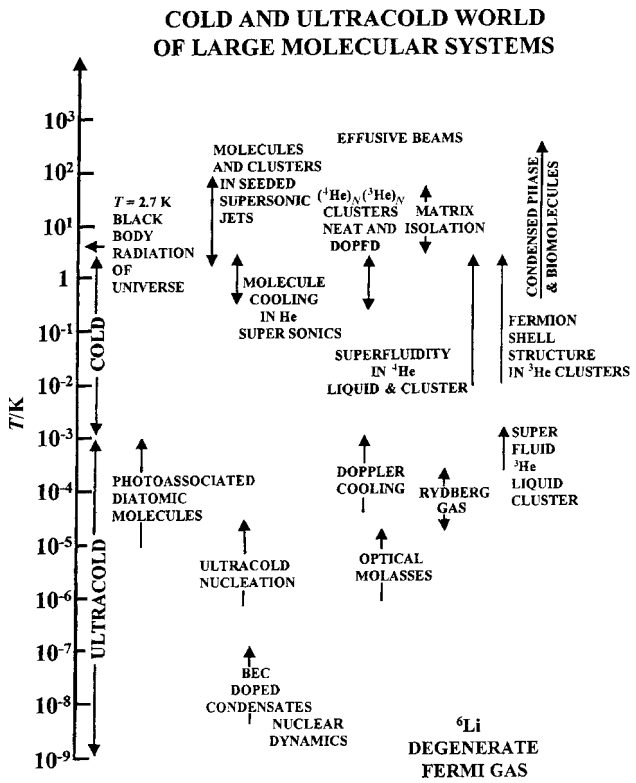


**Fig. 8** The world of cold and ultracold molecular and cluster systems.


## Acknowledgements

We are grateful to Dr Laurence Pruvost for fruitful collaboration on dynamics of optical molasses. This research was supported in part by the German–Israeli James Franck Program on laser–matter interactions.


## References


1 J. Jortner, *Z. Phys. D*, 1995, **24**, 247.
2 *Structure and Dynamics of Clusters*, ed. T. Kondow, K. Kaya and A. Terasaki, Universal Press, Tokyo, 1996.
3 J. M. Bonard and A. Chatelin, *Small Particles and Inorganic Clusters* (*ISSP 9*), Springer Verlag, Berlin, 1999.
4 Y. Imry, *Introduction to Mesoscopic Physics*, Oxford University Press, Oxford, 1997.
5 T. Walker, D. Sesko and C. E. Wieman, *Phys. Rev. Lett.*, 1990, **64**, 408.
6 D. W. Sesko, T. G. Walker and C. E. Wieman, *J. Opt. Soc. Am. B*, 1991, **8**, 946.
7 L. Pruvost, I. Serre, H. T. Duong and J. Jortner, *Phys. Rev. A*, 2000, **61**, 053408.

8 J. P. Toennies and A. F. Vilesov, *Annu. Rev. Phys. Chem.*, 1998, **49**, 1.
9 M. Hartmann, F. Mielke, J. P. Toennies, A. F. Vilesov and G. Benedek, *Phys. Rev. Lett.*, 1996, **76**, 4560.
10 M. Farnik, U. Henne, B. Samelin and J. P. Toennies, *Phys. Rev. Lett.*, 1998, **81**, 3892.
11 M. Rosenblit and J. Jortner, *Electron Bubbles in* $(^4He)_n$ *Clusters*, to be published.
12 S. Grebenov, J. P. Toennies and A. F. Vilesov, *Science*, 1998, **279**, 2083.
13 *Molecular Electronics*, ed. J. Jortner and M. A. Ratner, Blackwells, Oxford, 1998.
14 J. L. Bohn, B. E. Esry and C. H. Greene, *Phys. Rev. A*, 1998, **58**, 584.
15 F. Dalfovo, S. Giorgini, L. P. Pitaeskii and S. Stringari, *Rev. Mod. Phys.*, 1999, **71**, 462.
16 I. Last, I. Schek and J. Jortner, *J. Chem. Phys.*, 1997, **107**, 6685.
17 I. Last and J. Jortner, *Phys. Rev. A*, 2000, **62**, 13201.
18 R. E. Smalley, L. Wharton, D. H. Levy and D. W. Chandler, *J. Chem. Phys.*, 1978, **68**, 2487.
19 S. M. Beck, M. G. Liverman, D. L. Monts and R. E. Smalley, *J. Chem. Phys.*, 1979, **70**, 232.
20 D. H. Levy, C. A. Haynam and D. V. Brumbaugh, *Faraday Discuss. Chem. Soc.*, 1982, **73**, 137.
21 T. S. Zwier, M. Carrasquillo and D. H. Levy, *J. Chem. Phys.*, 1983, **78**, 5493.
22 C. A. Haynam, D. V. Brumbaugh and D. H. Levy, *J. Chem. Phys.*, 1984, **80**, 2256.
23 E. R. Bernstein, K. Law and M. Schauer, *J. Chem. Phys.*, 1984, **80**, 634.
24 C. A. Taatjes, W. B. Bosma and T. S. Zwier, *Chem. Phys. Lett.*, 1986, **128**, 127.
25 K. Yamanouchi, S. Isogai and S. Tsuchiya, *Chem. Phys.*, 1987, **116**, 123.
26 D. O. De Haan, A. L. Holton and T. S. Zwier, *J. Chem. Phys.*, 1989, **90**, 3952.
27 T. S. Zwier, *J. Chem. Phys.*, 1989, **90**, 3967.
28 D. H. Semmes, J. S. Baskin and A. H. Zewail, *J. Chem. Phys.*, 1990, **92**, 3359.
29 B. Coutant and P. Bréchignac, *J. Chem. Phys.*, 1994, **100**, 7087.
30 A. Bach, S. Leutwyler, D. Sabo and Z. Bacic, *J. Chem. Phys.*, 1997, **107**, 8781.
31 U. Even, J. Jortner, D. Noy, N. Lavie and C. Cossart-Magos, *J. Chem. Phys.*, 2000, **112**, 8068.
32 Y. Kwon and K. B. Whaley, *J. Chem. Phys.*, 2001, **114**, 3163.
33 A. Amirav, U. Even and J. Jortner, *Chem. Phys. Lett.*, 1979, **67**, 9.
34 R. P. Feynman and A. R. Hibbs, *Quantum Mechanics and Path Integrals*, McGraw Hill, New York, 1965.
35 R. S. Berry, in *Quantum Dynamics of Molecules*, ed. R. G. Wooley, Plenum, New York, 1980, p. 143.
36 E. Shalev, N. Ben-Horin, U. Even and J. Jortner, *J. Chem. Phys.*, 1991, **95**, 3147.
37 G. Vidali, M. W. Cole and W. H. Weinberg, *Phys. Rev. Lett.*, 1983, **51**, 118.
38 W. E. Carlos and M. W. Cole, *Surf. Sci.*, 1980, **91**, 339.
39 J. P. Toennies, W. Welz and G. Wolf, *Chem. Phys. Lett.*, 1976, **44**, 5.
40 E. Shalev and J. Jortner, *Chem. Phys. Lett.*, 1991, **117**, 161.
41 T. Lenzer and K. Luther, *J. Chem. Phys.*, 1995, **105**, 10944.
42 R. A. Aziz, F. R. W. McCourt and C. C. K. Wong, *Mol. Phys.*, 1987, **61**, 1487.
43 D. Fioretti, D. Comparat, A. Crubellier, O. Dulieu, F. Masnou-Seeuws and P. Pillet, *Phys. Rev. Lett.*, 1998, **80**, 4402.
44 R. Cote and A. Dalgarno, *Chem. Phys. Lett.*, 1997, **279**, 50.
45 I. Mourachko, D. Comparat, F. de Tomasi, A. Fioretti, P. Nosbaum, V. M. Akulin and P. Pillet, *Phys. Rev. Lett.*, 1998, **80**, 253.